JOURNAL OF SYNCHROTRON RADIATION
ISSN 1600-5775

Investigating structural aspects to understand the putative/claimed non-toxicity of the Hg-based Ayurvedic drug *Rasasindura* using XAFS

Nitya Ramanan,[a] Debdutta Lahiri,[a]* Parasmani Rajput,[b] Ramesh Chandra Varma,[c] A. Arun,[c] T. S. Muraleedharan,[c] K. K. Pandey,[a] Nandita Maiti,[d] S. N. Jha[b] and Surinder M. Sharma[a]

[a]High Pressure and Synchrotron Radiation Physics Division, Bhabha Atomic Research Centre, Purnima Labs Trombay, Mumbai, Maharashtra 400085, India, [b]Atomic and Molecular Physics Division, Bhabha Atomic Research Centre, Purnima Labs Trombay, Mumbai, Maharashtra 400085, India, [c]Arya Vaidya Sala, Kottakkal, Kerala 676503, India, and [d]Radiation and Photochemistry Division, Bhabha Atomic Research Centre, Trombay, Mumbai, Maharashtra 400085, India. *Correspondence e-mail: dlahiri@barc.gov.in

Received 3 February 2015
Accepted 29 June 2015

Edited by S. M. Heald, Argonne National Laboratory, USA

Keywords: Ayurvedic drug; XAFS; Hg; toxicity.

Supporting information: this article has supporting information at journals.iucr.org/s

XANES- and EXAFS-based analysis of the Ayurvedic Hg-based nano-drug *Rasasindura* has been performed to seek evidence of its non-toxicity. *Rasasindura* is determined to be composed of single-phase α-HgS nanoparticles (size $\sim$24 nm), free of Hg^0 or organic molecules; its structure is determined to be robust (<3% defects). The non-existence of Hg^0 implies the absence of Hg-based toxicity and establishes that chemical form, rather than content of heavy metals, is the correct parameter for evaluating the toxicity in these drugs. The stable α-HgS form (strong Hg—S covalent bond and robust particle character) ensures the integrity of the drug during delivery and prevention of its reduction to Hg^0 within the human body. Further, these comparative studies establish that structural parameters (size dispersion, coordination configuration) are better controlled in *Rasasindura*. This places the Ayurvedic synthesis method on par with contemporary techniques of nanoparticle synthesis.

1. Introduction

The discipline of Indian Ayurvedic medicine is distinctive in that it recognizes the therapeutic potency of heavy metals or their compounds when (i) mixed with organic molecules (herbs) and (ii) processed in a prescribed route employing natural products (Raha, 2013; Acharya *et al.*, 2014[1]). The advantages of Ayurveda over allopathic treatment include (i) cost-effectiveness (due to natural resources), (ii) longer shelf-life (due to the presence of metals) and (iii) minimized adverse side effects (Kumar & Gupta, 2011). In India, Ayurvedic medicine assumes crucial importance in bridging the gap between heavy patient load (rural/poor) and medical accessibility (Nandha & Singh, 2013). The scope of Ayurveda in India is aided by the availability of abundant medicinal plants (Raut *et al.*, 2013; Panghal *et al.*, 2010). Recognizing these facts, the Government of India (GOI) has taken keen interest in regularizing Ayurveda as a widespread alternative healthcare route. To practically realise this, the GOI has actively invested in Ayurvedic research at several institutes[2] with the objective of finding scientific evidence of the non-toxicity, standardization and effectiveness of Ayurvedic medicines (Valiathan, 2006; Bose & Saroch, 2012).

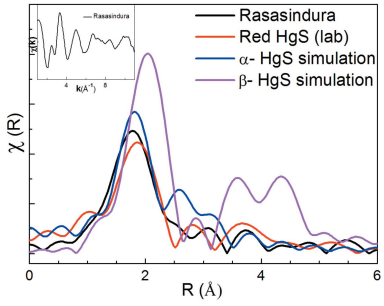

[1] See also http://www.ccras.nic.in/PharmacopoeialWork/Links/Compfom/AyurvedicFarmocopia.pdf.
[2] http://www.bhu.ac.in/ims/ayurveda/ayurveda_about.htm; http://www.ayurvedamanuscripts.com/; http://www.rria.nic.in/; http://www.nia.nic.in/?ref=12&id=6.

An objection raised against metal-derived drugs of Ayurveda (Patwabardhan, 2011; Baghel, 2013; Saper *et al.*, 2004; Leonti & Casu, 2013; Nishteswar, 2013) is the lack of scientific evidence for its claimed non-toxicity (Sarkar *et al.*, 2010; Kamath *et al.*, 2012; Panda & Hazra, 2012). Some reports suggest that toxicity is neutralized by compound formation (Tabakova *et al.*, 2006). However, their synthesis methods do not guarantee (nor experimentally prove) total elimination of the metallic phases or other toxic forms. In the absence of scientific validation, the present criterion of toxicity (or consequent ban) is defined by the metallic content (and not the chemical or structural forms) (Singh *et al.*, 2011).

The general Ayurvedic synthesis method ('Bhasmikaran') (Kumar *et al.*, 2006; Wadekar *et al.*, 2005) includes:

(i) Ingredients (metal + organic material). The advantages of metal (or its compounds) are manifold: longer shelf-life, small attainable sizes, quick drug release, lower required dosage, and size-controlled tunability of surface plasmon resonance for targeted drug delivery (Liao *et al.*, 2006).

(ii) Heating. The objective of heating is the formation of metal salts $[M^0 + B^0 \rightarrow M^+(B)^-]$; $B = S, O$ *etc.* The toxic reaction of elemental metals (M^0) within the body (C, H, O) proceeds by oxidation $[M^0 \rightarrow M^+(C, H, O)^-]$. This is curtailed by pre-forming stable $[M^+B^-]$ compounds before being administered into the body (Dubey *et al.*, 2009; Chaudhary, 2011; Mukherjee *et al.*, 2010[3]). Accomplishing 100% oxidation (zero M^0 remaining) is the most crucial step for non-toxicity of the drug.

(iii) Repeated purification. Impurities (*e.g.* toxic organic forms)/residual metals are removed by controlled heating for a prolonged period of time (Krishnamachary *et al.*, 2012).

(iv) Grinding. Reducing the particle size such that the end-product ('Bhasma') has a very fine texture (Bhasma) and no metallic shine (Patel, 1986; Shastry, 1979; Svoboda, 1998).

In modern perspectives, this process could be equivalent to the formation of metal–oxide (or compound) nanoparticles (Chakrapany & Singh, 2014; Sarkar & Chaudhury, 2010; Kulkarni *et al.*, 2013; Rastogi, 2010; Adhikari & Thapa, 2014; Paur *et al.*, 2011), that could act as drug-carriers in targeted drug delivery (Yonezawa *et al.*, 2000; De Jong & Barm, 2008).

As mentioned earlier, complete oxidation/removal of the toxic organic form and quality control of the 'Bhasma' particles have to be experimentally validated for Ayurvedic bhasmas to be credible and acceptable for use as drugs. Previous research includes reports on elemental analysis (Singh *et al.*, 2009), toxicology studies (Vardhini *et al.*, 2010), heavy metal bioaccessibility tests (Koch *et al.*, 2013) and X-ray diffraction (XRD) (Kamath *et al.*, 2012; Singh *et al.*, 2009). However, none of them could unambiguously establish *complete* oxidation status or account for non-toxicity. In this work, we propose to accomplish this by X-ray absorption fine-structure (XAFS) investigation of the structure and chemical form of α-HgS-based *Rasasindura*. The latter is widely prescribed (<125 mg per day) for treatment of certain diseases (Varier, 1999; Gokarn *et al.*, 2012; Patgiri & Gokarn, 2014; Mahdihassan, 1987; Ingole, 2013; The Ayurvedic Formulatory of India, 2003). Recent *in vivo* experiments (Anita *et al.*, 2013; Dwivedi *et al.*, 2012, 2013, 2014; Kanojia *et al.*, 2013) have established the therapeutic effect of *Rasasindura* and ruled out toxicity. We clarify that our XAFS understanding/validation of non-toxicity will cover only the *virgin* medicine, *i.e. before* being administered into body. How it reacts within the body or remains non-toxic within the body is beyond the scope of this work. Systematic biochemical experiments are required to answer these questions.

XAFS is an oscillatory feature above the absorption edge of the constituent atom, resulting from the interference between the outgoing photoelectron wave and the backscattered wave from the surrounding atoms. By analyzing the period and amplitude of these oscillations, one can obtain detailed structural information around the excited atom. One can selectively excite different atomic species in the material (by tuning the incident X-ray energy around their binding energies) and obtain site-resolved structural information (Koningsberger & Prins, 1988). This element-specificity makes XAFS more sensitive to small amounts ($\geq$3%) of defects/hidden phases that are not detected by XRD. Further, the region close to the edge of the XAFS spectrum is called XANES (X-ray absorption near-edge structure) and contains information about the oxidation state (single or multi-valence) (Koningsberger & Prins, 1988).

As mentioned above, elemental specificity of XAFS yields better-resolved results than XRD. In this case: (i) in the backdrop of the primary α-HgS phase there could be minute quantities of segregated unstable and toxic chemical phases (pure Hg, β-HgS, organic Hg compound) that are undetected by XRD; (ii) identification of possible core-shell structure of the nanoparticles; (iii) surface segregation (if any) for the nano-crystals; and (iv) identification of local defects (pores *etc.*)/disorder *etc.* within the nanoparticle. Each of these parameters, as explained later, is correlated with the toxicity or efficacy of drug delivery/action.

1.1. HgS-based *Rasasindura*

Due to high mobility, water-solubility and relative ease of oxidation[4], metallic mercury (Hg^0) is one of the most toxic elements known to humans; it interacts with the human body to form toxic methyl-mercury $[(CH_3)Hg]$[5]. While there is worldwide concern against Hg contamination in food/water/soil (Azimi & Moghaddam, 2013; Wang *et al.*, 2004; Zhang & Wong, 2007; Mercury Study Report to Congress, 1997[6]), it is strange that Hg-based medicines are recommended in Ayurveda, often in concentrations larger than the WHO-permissible limit (>1 p.p.m.)[7]. From reported XRD results, the crystal structure of *Rasasindura* is known to be α-HgS. Preli-

[3] See also http://www.slideshare.net/technoayurveda/bhasma-nano.

[4] http://web.anl.gov/PCS/acsfuel/maroto-valer.pdf; http://copublications.greenfacts.org/en/dental-amalgam/l-3/4-health-effects-amalgams.html.

[5] http://www.cfspages.com/mmercmicro.html.

[6] See also http://www.epa.gov/hg/eco.htm; http://www.usgs.gov/themes/factsheet/146-00/;http://www.cseindia.org/node/439.

[7] http://pib.nic.in/newsite/erelease.aspx?relid=42213; http://www.udel.edu/chem/C465/senior/fall00/Mercury/health.htm.

minarily, the non-toxicity of *Rasasindura* can be correlated with the advantageous properties of bulk α-HgS (Frawlay, 2000):

(i) Hg has a special affinity for S (Wiberg & Wiberg, 2001), resulting in the formation of a strong Hg—S bond. This is supported by recent experiments on Hg-contaminated soil samples (Mishra *et al.*, 2011), where it was observed that binding of Hg^{2+} with sulfur-containing groups (rather than oxygen-containing group) significantly arrests its reduction ($Hg^{2+} \rightarrow Hg^{0}$).

(ii) Low solubility and bioavailability (Koch *et al.*, 2013) (0.001 g L^{-1}) of α-HgS results in a low accumulation in the human body (0.2% is absorbed in the gastrointestinal tract and only 0.02% reaches the kidneys) (Sin *et al.*, 1989; Yeoh *et al.*, 1986).

(iii) Toxicity [HgS] $\simeq 10^{-4} \times$ Toxicity [(CH_3)Hg] (Chuu *et al.*, 2007; Huang *et al.*, 2012; Liu *et al.*, 2008).

(iv) The possibility of HgS $\rightarrow$ (CH_3)Hg conversion by human intestinal bacteria has been ruled out (Zhou *et al.*, 2011).

However, these advantages of α-HgS may not hold good in nanoparticle form (Bhasma), *i.e.* for α-HgS nanocrystals: (i) surface energetics, increased strain and vacancy defects (Deneen & Carter, 2006; Perrey *et al.*, 2005) may lead to the formation of local Hg^{0} sites, *i.e.* initiate the reverse reaction [$Hg^{2+} \rightarrow Hg^{0}$]. (ii) Increased disorder/strain can disintegrate the nanoparticle into toxic forms; therefore, robustness of the nanoparticle is of additional concern. (iii) Further, XRD cannot unambiguously rule out the presence of <5% Hg^{0} or organic Hg due to its limited resolution. To validate the reported non-toxicity of *Rasasindura*, we need to establish reliably that *Rasasindura* has (i) complete absence of the unstable and toxic chemical forms, *viz.* Hg^{0}, β-HgS and organic Hg, and (ii) a robust nano-structure with minimal defects.

1.2. Synthesis method

Rasasindura, like any other licensed and standardized formulation, is subjected to standard operating procedures, including starting/in-process/finishing quality-control checks. *Rasasindura* was prepared by Arya Vaidya Sala (India) following three distinct steps. (i) Pre-treatment of Hg and S with herbal and milk products: Hg was ground with slaked lime on a mortar for three days and filtered through a fine cloth. The filtrate was ground with garlic and rock salt until it turned black in color and was then washed in water (Sharma, 1979*a*). S was heated with ghee and allowed to drop through a cloth into milk. The resultant granules were collected and washed with water (Sharma, 1979*b*). (ii) Mixing of Hg and S [Hg:S = 1:1] along with other herbal ingredients (Aloe vera juice) and ground for five days using an electric grinder, resulting in the formation of black-HgS (*Kajjali*) (Sharma, 1979*c*). (iii) Thermal treatment at 600°C of dried *Kajjali*, in porcelain pots, with porcelain lid and totally covered with seven layers of clay-smeared cloth. The whole pot is smeared with clay for total sealing. The pots are placed into an open hearth furnace (electrically operated) for 24 h with the temperature being raised from room temperature to 600°C. After 24 h, heating is cut off and the pots are allowed to cool down naturally for the next 24 h. The cooled porcelain pots are opened by cutting open the clay seal. The final product, *Rasasindura*, in the form of fine dust of brick red colour, will be found deposited on the inside roof of the porcelain lid, and is then scraped off (Hariprapannaji, 2004). It is triturated in a mortar and pestle and then passed through a fresh nylon cloth of 200 mesh.

Schematically, the entire synthesis process can be thus summarized:

$$\begin{aligned}[(\mathrm{Hg}) + (\mathrm{S})] &\rightarrow \textit{Kajjali}\ (\text{black-HgS}) \\ &\rightarrow \textit{Rasasindura}\ (\text{red-HgS}).\end{aligned}$$

For HgS formation, S + Hg $\rightarrow$ HgS, $\Delta G^{0} = -46$ kJ mol^{-1}. The negative free energy change ΔG^{0} shows the feasibility of formation of some amount of HgS even before heat treatment of *Kajjali* (Svensson *et al.*, 2006). Heat treatment of *Kajjali* is essential to decrease the proportion of unreacted S, and the herbal ingredients provide the acidic medium (catalyst) required for this reaction besides aiding in solidification of Hg (Singh *et al.*, 2009).

To understand the relative stability and non-toxicity of *Kajjali* and *Rasasindura*, we studied their inorganic counterparts (*viz.* black- and red-HgS).

1.3. Inorganic black-HgS and red-HgS

In bulk form, black- and red-HgS generally represent the two structural forms of (inorganic) HgS.

(*a*) Symmetry. In bulk form, black- and red-HgS represent structural polymorphs, *viz.* cubic β-HgS (tetrahedral) and trigonal α-HgS (octahedral), respectively.

(*b*) Stability. Black-HgS is unstable below 600 K (Rickard, 2012), decomposes into red (α)-HgS, and is prone to oxidation. The instability of black-HgS may be due to the poor packing efficiency of the tetrahedral configuration (Karkare & Bahuguna, 2007).[8] On the other hand, red (α)-HgS is reported to be stable (Bhuse, 2011) because of its significantly enhanced packing efficiency. The smaller misfit factor for the octahedral configuration in red (α)-HgS can be accommodated with a slight distortion of the octahedron and phase-stabilized. In summary, α-phase $\rightarrow$ stability $\rightarrow$ non-toxicity.

(*c*) Toxicity. Red (α)-HgS, the stable structural form, has *not* been explicitly reported as toxic in the literature (De, 2009[9]).

$$\text{Toxicity}\,[\text{red}(\alpha)\text{-HgS}] \simeq 10^{-4} \times \text{Toxicity}\,[(\mathrm{CH_3})\mathrm{Hg}]$$

(Chuu *et al.*, 2007; Huang *et al.*, 2012; Liu *et al.*, 2008). On the other hand, there are several reports on black-HgS being toxic (Morris, 1992[10]).

[8] Packing fraction $PF_{\beta\text{-HgS}} = 32\%$; $PF_{\alpha\text{-HgS}} = 58\%$.
[9] See also http://www.mercurynetwork.org/uk/wp-content/uploads/2009/11/Orthiel.pdf; http://www.hallegeologicalservices.ca/?p=692.
[10] See also http://www.lookchem.com/Mercury-II-sulfide/; http://www.answers.com/topic/mercuricsulfide; http://www.instruments-support/labs-facilities/chemistry-laboratories/list-of-chemicals/dangerous-chemicals.ill.eu/.

1.4. Pre-XAFS characterization of *Rasasindura*

Although colors are strong indicators of structural forms, they could be elusive in this case since Bhasma samples are formed of nano-sized particles where color could be size-dependent. To obtain a comprehensive overview of the *Rasasindura* structure (with reference to laboratory-based α-HgS nanoparticles, which we refer to as 'red-HgS' hereon), we have employed complementary techniques: XRD/X-ray fluorescence (XRF)/Fourier transform (FT) Raman and IR/surface enhanced Raman scattering (SERS). XRD and XRF experiments were performed at the Indus-2 synchrotron source (India), where high-resolution information could be extracted due to the very high photon flux (~10^{11} photons s^{-1}). SERS, FT-Raman and FT-IR spectra were recorded at Bhabha Atomic Research Centre (India). The conclusions from these techniques, listed in Table 1, unanimously establish that *Rasasindura* has the same structure as red (α)-HgS and, additionally, is better ordered.

Table 1
Characterization of *Rasasindura* and red-HgS.

Technique		*Rasasindura*	Red-HgS (lab)
XRD (Fig. S1)	Form	α-HgS; no Hg^0/organo-HgS phase detected	α-HgS; no Hg^0/organo-HgS phase detected
	Shape	Spherical	Spherical
	Particle size	24 nm	18 nm
XRF (Fig. S2)	Elements	Hg, S and Zn (0.6%) (Note that Zn is reportedly found as impurity in Hg)	Hg, S and Zn
	Hg:S ratio	1:1	1:1
FT-Raman (Fig. S3)	Form	α-HgS	α-HgS
	Bonding	Strong Hg—S bond	Strong Hg—S bond
	Order	Better ordered	
SERS (Fig. S4)	Surface organic groups	Absent	Absent
FT-IR	Organic groups	Absent	Absent

2. XAFS experimental details

For XAFS experiments, *Rasasindura* was ground to a fine powder using mortar and pestle. The ground powder was mixed with AR-grade isopropyl alcohol in a beaker and the solution was allowed to stand undisturbed for 40 min. During this procedure, the larger particles settled down while the smallest particles remained in solution. The solution was decanted into a petri dish and left to evaporate overnight. The alcohol evaporated, leaving behind fine (~5 µm-diameter) particles (Lahiri, 2016). 20 mg of these particles was mixed with 80 mg of cellulose and pressed into a 15 mm-diameter pellet, which was used for recording XAFS data.

Transmission-mode XAFS was recorded on *Rasasindura* and red (α)-HgS at the Hg L_3-edge (12.284 keV) at the Scanning EXAFS beamline (BL-09), Indus-2 Synchrotron Radiation Source, RRCAT (India). A pair of Si(111) crystals in parallel geometry was used as a double-crystal monochromator (DCM). A 1.5 m-long horizontal pre-mirror with meridional cylindrical curvature was used to obtain a collimated beam on the first crystal of the DCM and reject higher harmonics from the XAFS spectrum. Incident and transmitted intensities were measured using N_2/Ar-filled ionization chambers.

XAFS data were processed using *ATHENA* software. The extracted XAFS oscillations, $\chi(k)$, were Fourier-transformed into real space $\chi(R)$ for fitting. $\{k = [2m(E - E_0)/\hbar^2]^{1/2}$ where m is the electron mass and E_0 is the edge energy of the relevant absorption edge.} XAFS oscillations in k- (inset) and R-space are shown in Fig. 1. A structural model was constructed using *FEFF6.1* (Newville *et al.*, 1995). The model parameters were allowed to vary while fitting (using *FEFFIT*) to yield the best-fit values for bond lengths (R), coordination numbers (N) and Debye–Waller factors (DWF or σ^2). The R-factor was considered as an estimate of the quality of fit (Newville *et al.*, 1995; Newville, 2001).

3. Results and discussion

XAFS data for *Rasasindura* and laboratory-produced red (α)-HgS were fitted for k = 2.8–8.6 Å^{-1}; R = 1.1–3.4 Å. The limited k-range is due to (i) smearing of the Hg XAFS signal by the high core-hole lifetime of Hg, (ii) large disorder of higher shells (as shown later) and (iii) fast decay of oscillations from low-Z (sulfur) backscattering neighbours. EXAFS modelling

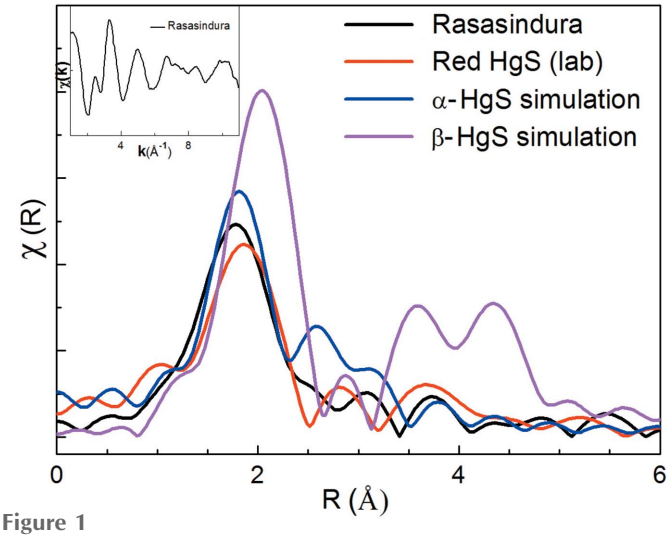

Figure 1
Comparison of the Hg L_3-edge XAFS data on *Rasasindura* and red (α)-HgS with simulated XAFS data for α- and β-HgS. It is clear that the data for *Rasasindura* resemble α-HgS (not β-HgS). The inset shows the $\chi(k)$ data for *Rasasindura*.

was essentially limited to Hg—S fitting for which k = 2.8–8.6 Å^{-1} is more than sufficient. In order to reduce error bars and have a sufficient number of points for fitting, simultaneous fitting of the data was carried out for different k-weights of the transform, *viz.* $\int k^w \chi(k)$; w = 0, 1. Some of the ripples observed in Fig. 1 are due to truncation effects from the limited data range and do not represent real data. Apparently, features around 2.5–3 Å (Fig. 1) look less sharp for *Rasasindura*. However, it should not be mis-interpreted as higher disorder; as we note from the analysis results (described below), Hg—S bond lengths in *Rasasindura* are displaced relative to each other such that their scattering contributions phase cancels. In fact, *Rasasindura* is found to be better ordered [than red (α)-HgS] from our analysis.

3.1. Phase segregation

Since changes in XANES (inset of Fig. 2*a*) are very subtle between α-HgS (Hg^{+2}), Hg^0 and *Rasasindura*, we have plotted derivatives of their XANES spectra (Patty *et al.*, 2009; Colombo *et al.*, 2013) in Fig. 2(*a*). XANES derivative features for *Rasasindura*, *viz.* pre-edge (*A*) and edge position (*B*), resemble α-HgS (Hg^{+2}) (Fig. 2*a*) and are markedly different from Hg^0 (*C*). A comparison of XANES derivative spectra of HgS compounds (*Rasasindura,* α-HgS) and Hg^0[11] clearly reveals (i) a shift in the edge position (*B*) towards higher energy (E_{shift} = 5 eV) for *Rasasindura,* α-HgS, due to higher oxidation state (+2), and (ii) the presence of a pre-edge feature (*A*) in HgS due to S (2*p*)–Hg (6*d*) orbital hybridization, which is absent in Hg^0. The main absorption edge (*B*) corresponds to an intra-site Hg (2*p*) → Hg (6*d*) transition, consistent with the dipole selection rule ($\Delta l = \pm 1$). While direct inter-site Hg (2*p*) → S (2*p*) transition is prohibited by the dipole rule, the pre-edge feature (*A*) is an indirect signature of the transition to S (2*p*) through Hg (6*d*)–S (2*p*) hybridization. Strong pre-edge (hybridization) features confirm strong Hg—S covalent bonds.

Our next objective is to determine whether Hg^0 is *completely* absent or *partially* present. Since our XRD spectrum does not show a signature of the Hg^0 phase, one can presume that the Hg^0 content (x) would be <5%. On the other hand, XANES derivative spectra show that the amplitudes of the (*A*, *B*) peaks and their ratio (*X*) are significantly reduced,

$$\begin{pmatrix} \Delta A \\ \Delta B \\ \Delta X \end{pmatrix} = \begin{pmatrix} -33\% \\ -25\% \\ -17\% \end{pmatrix},$$

in *Rasasindura* (X = 1.2) with respect to α-HgS (X = 1.5). Since peak *A* (α-HgS) is negatively correlated with peak *C* (Hg^0), a mixture of these phases (Hg^0, α-HgS) could reduce the net amplitude around peak *A* and subsequently reduce *X* (as observed for *Rasasindura*). This implies that the reduced features of the *Rasasindura* spectra could be consistent with the co-existence of (Hg^0, α-HgS) phases. To clarify this ambiguity, we simulated the derivative spectra for different fractions (x_{Hg^0}) of Hg^0 (Fig. 2*b*). For x_{Hg^0} = 0 → 30%, the

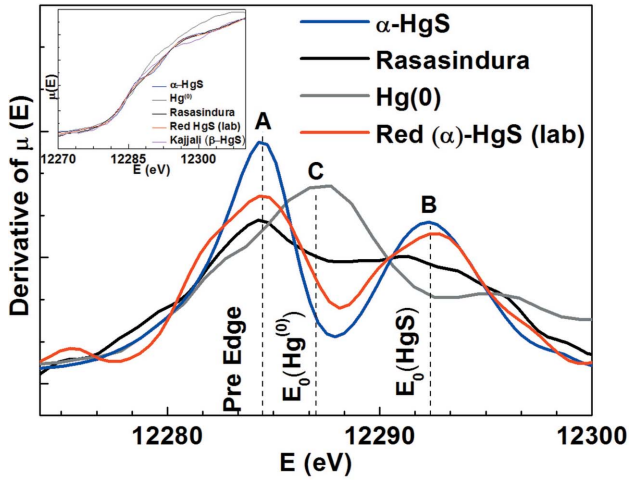

(*a*)

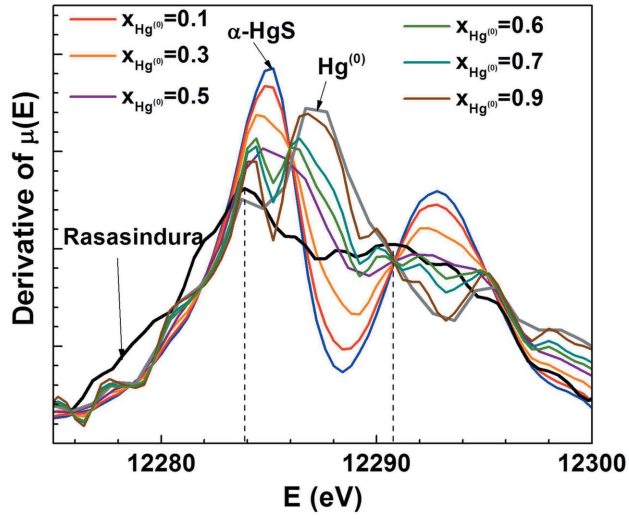

(*b*)

Figure 2
Comparison between (*a*) derivatives of XANES data on α-HgS, Hg^0, *Rasasindura* and red (α)-HgS (lab). *Rasasindura* closely resembles α-HgS and red (α)-HgS (lab). Clearly in *Rasasindura*, (i) the edge position is shifted with respect to Hg^0 (E_{shift} = 5 eV) and (ii) pre-edge features are present which are absent in Hg^0. The inset shows a comparison between XANES spectra for α-HgS (Hg^{+2}), Hg^0 and *Rasasindura*. Since the observed changes are subtle, we compared the derivatives of the respective XANES spectra. (*b*) Simulated derivative spectra for different fractions (x_{Hg^0}) of Hg^0.

amplitudes of the (*A*, *B*) peaks are progressively dampened while their ratio (X = 1.5) remains constant. For $x_{Hg^0} \geq 30\%$, the signature of Hg^0 becomes dramatically conspicuous as the spectra evolve into peaks *A*′, *C*′ following peaks *A*, *C*; peak *B* is completely dampened. With increasing Hg^0 content, the positions of *A*′, *C*′ move away from and towards *A*, *C*, respectively, such that the split becomes wider. The spectrum of *Rasasindura* is not consistent with any of these mixed-phase features; instead, X = 1.3 resembles XANES for Hg—S bonds in soil, water, *etc.* (Patty *et al.*, 2009; Myneni *et al.*, 2009; Colombo *et al.*, 2014; Huggins *et al.*, 2009; Rajan *et al.*, 2008[12]). Further, XANES for *Rasasindura* is inconsistent with organo-

[11] http://ftp.esrf.eu/pub/UserReports/44815_B.pdf.

[12] See also http://doesbr.org/PImeetings/2012/pdf/Tues/NagySBR2012.pdf.

Table 2
Comparison of bond lengths (R).

	Hg—S1	Hg—S2	Hg—S3	Hg—Hg1	Hg—Hg2	Hg—Hg3
α-HgS (theory)	2.36 Å	3.1 Å	3.3 Å	3.79 Å	4.09 Å	4.14 Å
Red (α)-HgS (lab) (XAFS)	2.36 Å	3.10 Å	3.30 Å	Absent		
Rasasindura (XAFS)	2.34 (2) Å	3.02 (4) Å	3.31 (5) Å	Absent		

Hg (Colombo *et al.*, 2013). Reconciling XRD and XANES results, we unambiguously conclude that Hg^0 and organo-Hg are absent in *Rasasindura*.

Compiling XANES and SERS results, we confirm that the chemical form of *Rasasindura* is single-phase α-HgS; the absence of unstable and toxic chemical forms (Hg^0, β-HgS, organic Hg) is the most significant evidence towards confirming the non-toxicity of *Rasasindura*.

3.2. Crystalline structure details and degree of disorder

In Fig. 1, we compared *Rasasindura*/red (α)-HgS data with simulations for α-HgS and β-HgS crystal structures. Except for larger disorder, near-neighbor features (R < 2.5 Å) of both *Rasasindura* and red (α)-HgS clearly resemble α-HgS (in terms of peak position). Theoretical bond lengths for α-HgS are shown in Table 2. XAFS fit results (Fig. 3*a*) confirm the α-HgS configuration for S neighbors. Our bond length and coordination number results for Hg—S bonds are consistent with the reported literature (Charnock *et al.*, 2003; Manceau & Nagi, 2008). [Other models (*a*) cubic = 6S, (*b*) β-HgS = 4S (R = 2.53 Å) yielded poor quality fits.] From Fig. 3(*a*) we observe that the Hg—S near-neighbor configuration is better ordered (lower σ^2) in *Rasasindura* compared with laboratory-synthesized inorganic red (α)-HgS. An example of the quality of fit is shown in Fig. 3(*b*).

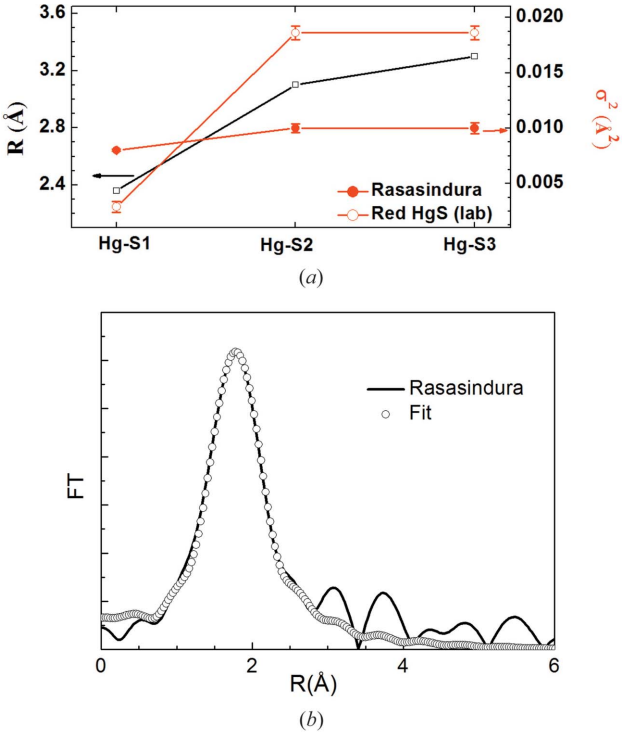

Figure 3
(*a*) XAFS fit results for *Rasasindura* and red (α)-HgS (lab). *Rasasindura* is more ordered than red (α)-HgS (lab). (*b*) Comparison of data with fit for *Rasasindura*.

In contrast, the Hg—Hg bond features (R > 2.5 Å) of α-HgS are conspicuously absent in the experimental XAFS spectra (Charnock *et al.*, 2003; Kim *et al.*, 2004) [although the XRD-generated radial distribution function (using *RAD* software) (Petkov, 1989) clearly reproduces the Hg—Hg peak]. XAFS and XRD experimental results can be reconciled by considering the possible role of the Hg—Hg disorder (σ^2_{Hg-Hg}). By simulating XAFS for different σ^2_{Hg-Hg}, we determined the critical disorder value for the Hg—Hg peak suppression to be $\sigma^2_{Hg-Hg} \geq 0.025$ Å^2 (see Fig. S5*a* of the supporting information). Independently, we simulated XRD patterns with different values of σ^2_{Hg-Hg}. The XRD pattern for *Rasasindura* is insensitive to σ^2_{Hg-Hg} variation up to σ^2_{Hg-Hg} = 0.035 Å^2 (Fig. S5*b*). From XAFS and XRD simulations, we thus conclude and clarify that the apparent 'absence' of Hg—Hg correlation features in the experimental XAFS spectrum is actually a reflection of the large disorder in Hg—Hg bonds. Despite Hg being the heavier atom, $\sigma^2_{Hg-Hg} \gg \sigma^2_{Hg-S}$ due to a strong Hg—S covalent bond and relatively weak van der Waal interaction between Hg—Hg. The HgS structure can be depicted as spiral –S—Hg—S—Hg—S– chains (Fig. S6*a*), in which Hg—S and Hg—Hg bonds are intra- and inter-chain, respectively. Any defect in the spiral (*e.g.* compression/elongation) affects the inter-chain Hg—Hg bond substantially while the strong Hg—S bond remains largely unaffected (Fig. S6*b*). This leads to $\sigma^2_{Hg-Hg} > \sigma^2_{Hg-S}$.

3.3. Analysis of the nanocrystal units

For D_{Rasa} = 24 nm, the surface–volume ratio of atoms is ~2% (*i.e.* $x_{Hg}^{Surface}$ = 2%). The XAFS coordination result N_{Hg-S} = 6 (±3%) is the site-averaged contribution from core (x_{Hg}^{Core} = 98%) and surface ($x_{Hg}^{Surface}$ = 2%) sites. Considering coordination loss (ΔN) due to truncation at a bare surface, the net (theoretical) coordination for a particular bond length (R = Hg—S in this case) (Calvin *et al.*, 2003):

$$N_{nano}(Hg-S) = \left[1 - \frac{3}{4}\left(\frac{2R}{D}\right) + \frac{1}{16}\left(\frac{2R}{D}\right)^3\right] N_{BULK}$$
$$\approx 6\ (\approx N_{expt}),$$

i.e. $\Delta N_{D=24\,nm} \approx 2\%$, which is less than the XAFS resolution (ΔN = ±3%). Thus, our XAFS coordination result is appar-

ently consistent with the theoretical size-dependent coordination loss for a chemically homogeneous defect-free nanocrystal. Any defect, if present, has to be accommodated within a 3% error bar of the XAFS coordination result. We provide defect estimates that are consistent with this constraint.

(*a*) Vacancy. Vacancy-induced extra coordination loss is not observed; one can rule out the presence of a (≥3%) vacancy in the nanoparticles.

(*b*) Surface segregation of Hg. Due to an insignificant surface–volume ratio (2%), the surface contribution to the XAFS coordination result is insignificant; hence, XAFS results do not reflect the surface coordination unambiguously. [We have calculated the critical core size ($D_{\rm core} \leq 4$ nm) for resolving surface coordination.] To estimate the possibility (and fraction) of preferential surface site occupancy by Hg, we considered the chemical non-uniformity across the nanocrystal and allowed $x_{\rm Hg}^{\rm Surface}$:$x_{\rm Hg}^{\rm Core}$ to vary (instead of constraining $x_{\rm Hg}^{\rm Surface} = 2\%$). By re-calculating the site-averaged Hg coordination as a function of $x_{\rm Hg}^{\rm Surface}$, we determined that $x_{\rm Hg}^{\rm Surface} < 6\%$ is consistent with the XAFS result.

(*c*) Organic molecules at the surface. Due to an insignificant surface–volume ratio and weak backscattering factor of organic elements, XAFS was unable to unambiguously detect the presence of surface organic molecules. We obtained the answer by employing SERS. SERS results convincingly ruled out the presence of organic molecules at the surface. This is remarkable since the Ayurvedic synthesis method involves organic molecules. We believe that organic molecules were removed during purification steps or heating.

(*d*) Porosity. To explore the presence of nano-pores (cylindrical) in the particle, we theoretically estimated the average coordination for pore parameters $D_{\rm p}$, $H_{\rm p}$, $N_{\rm p}$; $D_{\rm p}$ = pore diameter, $H_{\rm p}$ = pore-height, $N_{\rm p}$ = number of pores. By varying one of these parameters, $H_{\rm p}$ = 1–10 nm (*i.e.* $H_{\rm p}^{\rm max}$ = radius of the nanocrystal), we determined the range of $(D_{\rm p}, N_{\rm p})_{H_{\rm p}}$ (*i.e.* for each $H_{\rm p}$) that is consistent with $N_{\rm expt} \approx 6$ (±3%). Compiling all these calculation results, we obtained $D_{\rm p}^{\rm max} = 10$ nm, $N_{\rm p}^{\rm max} = 20$, $V_{\rm p}^{\rm max} = 7\%$. [Note that $(D_{\rm p}, N_{\rm p})_{H_{\rm p}}$ are negatively correlated.] $V_{\rm P}^{\rm max} = 7\%$ implies that pores occupy a small volume fraction of the nanocrystal, which is insufficient to generate large disorder and helps preserve the robust character of the nanoparticle. Minimal defects for these nanocrystals could be correlated with prolonged annealing and large particle size ($D_{Rasa} \approx 24$ nm). Interfacial defects and broadening generally increase significantly for $D \leq 8$ nm (Shibata *et al.*, 2002; Chaudhuri & Paria, 2012; Alayoglu *et al.*, 2009).

[Note that the above conclusions for *Rasasindura* also hold good for red (α)-HgS due to similar nanoparticle size and coordination results.] These pores could provide the pathway for drug binding.

A summary of the nanocrystal coordination analysis is the presence of a robust and chemically homogeneous (α-HgS) nanocrystal (Fig. 4). Including the error bar ($\Delta N = \pm 3\%$), we could accommodate possible defects in the particle (*viz.* vacancy, surface segregation, nano-pore) and determine the upper limit of their content: <3–7%.

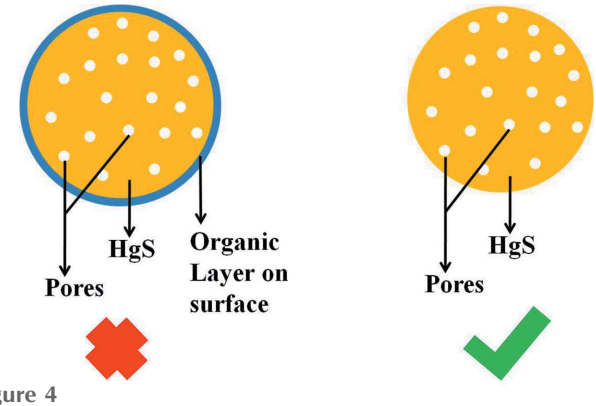

Figure 4
Model of a *Rasasindura* nanocrystal with 24 nm HgS core.

3.4. Implications of our structural results for toxicity and synthesis route

3.4.1. Toxicity. For successful non-toxic functioning of heavy-metal-based Ayurvedic medicine, the most crucial factors (with respect to toxicity) are: (i) no organic chemical form of metal (Hg) and complete oxidation of metals (no remnant of Hg^0 metallic state) before entering the human body; (ii) integrated structure of the medicine so that the compound form is retained inside the body (no reduction to metallic form).

From our work, we observe that both criteria are met for *Rasasindura*. Our XANES/SERS/EXAFS results unanimously establish that *Rasasindura* is in the single-phase α-HgS stable form; unstable and toxic forms of Hg, *viz.* metallic Hg^0 [*i.e.* Hg is completely oxidized], β-HgS and organic complex of Hg, are absent. Our structural results unanimously establish that *Rasasindura* is composed of robust (minimal defects) single-phase α-HgS nanoparticle units ($D_{Rasa} \approx 24$ nm).

As already mentioned above, α-HgS is non-toxic which implies the same for *Rasasindura*. The stable α-phase form and robust character of the nanoparticle would help to maintain its integrity during the entire drug delivery process (Yoshitomi *et al.*, 2009). Cinnabar, being one of the most stable and non-reactive classes of compounds addressing toxicity issues related to engineered nano-material is not particularly relevant in this case.

3.4.2. Synthesis. We compared the structures of *Rasasindura* and red-HgS, *i.e.* end products of organic and inorganic synthesis methods. Interestingly, we found that the particle size distribution is better controlled in *Rasasindura*.[13] The distribution is Gaussian, with size $\sigma_D^{Rasa} = 3.5$ nm and dispersion = 18%. On the other hand, the size-distribution of red (α)-HgS is non-Gaussian ($D_{\rm peak} \simeq 20$ nm) and heavily skewed towards higher particle sizes; the total size distribution spreads over $\Delta D = 50$ nm. The better size control in *Rasasindura* could be due to herbal coating, similar to the modern-day surfactant-mediated nanoparticle synthesis and sublimation process at the final stage. The coordination configuration for both show large disorder for Hg—Hg bonds but well

[13] Transmission electron microscope result provided by Professor Sujit Roy, IIT-Bhubaneswar.

defined Hg—S bonds. The Hg—S coordination distribution is better ordered in *Rasasindura* (Fig. 3) which could be due to prolonged annealing.

The efficacy of drug delivery and action is directly affected by particle size, size distribution and order (Tiwari & Tiwari, 2013). Size (and size distribution) can determine the *in vivo* distribution, biological fate, toxicity and targeting ability of these delivery systems. Although the implications of size ($D_{Rasa} \simeq 24$ nm) are not clear at the moment, we would like to cite the correlation between nano-drug and target cell sizes, as in targeted drug delivery (optimal particle size requirement is target specific) (Walkey *et al.*, 2009; Smith *et al.*, 2013; Niikura *et al.*, 2013). Why Ayurvedic α-HgS (*Rasasindura*) rather than inorganic α-HgS nanoparticle (red HgS) is therapeutic could be related to their difference in size distribution; larger red-HgS particles (30–70 nm) may be failing to penetrate cells and thus be less effective. Further, the better ordered structure (and consequently predictable electronic structure) of *Rasasindura* can help maintain better equilibrium within the body.

Thus, our work not only helps to understand the non-toxicity of *Rasasindura* but also establishes the Ayurvedic synthesis method for a well controlled end-product.

4. Conclusion

We have employed XAFS (coupled with supporting techniques) to investigate the structure of *Rasasindura*. The main results are that *Rasasindura* has the same structure as non-toxic α-HgS, and toxic chemical forms, *viz.* elemental Hg^0, organo-Hg, are completely absent. Our results also demonstrate that the nanocrystal ($D_{Rasa} \approx 24$ nm) units of *Rasasindura* are robust, defect-free and free of organic molecules. The absence of these toxic chemical forms helps in the understanding of non-toxicity, and the robust character implies the nanoparticle integrity during drug release. Further, we observed that Ayurvedic synthesis yielded a better controlled end-product than laboratory-based red (α)-HgS: lower size dispersion and better ordered coordination configuration. With all these advantages, *Rasasindura* can be considered a potential therapeutic agent for target cell sizes ($\sim$24 nm).

Acknowledgements

We deeply thank Dr M. S. Valiathan and Dr R. Chidambaram for initiating us into the project. We sincerely thank Dr Ketaki Bapat for her guidance. We thank our collaborators for supplementary techniques: Mr A. K. Singh and Dr M. K. Tiwari (XRF; RRCAT); Mr S. R. Vishwakarma, Mr Himal Bhatt and Dr M. N. Deo (FT-Raman and FT-IR; BARC); Dr Sudhir Kapoor (SERS; BARC).

References

Acharya, P., Ranjan, R., Kirar, P., Srivastva, S. & Singh, P. (2014). *Ind. J. Adv. Plant Res.* **1**, 18–20.
Adhikari, R. & Thapa, S. (2014). *Adv. Exp. Med. Biol.* **807**, 23–32.
Alayoglu, S., Zavalij, P., Eichhorn, B., Wang, Q., Frenkel, A. I. & Chupas, P. (2009). *Nano*, **3**, 3127–3137.
Anita, K., Anita, S., Venketeswalu, V. & Kumar, G. V. (2013). *Int. Ayur. Med. J.* **1**, 1–6.
Azimi, S. & Moghaddam, M. S. (2013). *Environ. Ecol. Res.* **1**, 12–20.
Baghel, M. S. (2013). *Ayu*, **34**, 2–3.
Bhuse, V. M. (2011). *Arch. Appl. Sci. Res.* **3**, 339–349.
Bose, A. & Saroch, V. (2012). *Intl J. Pharm. Res. Biol. Sci.* **1**, 96–119.
Calvin, S., Miller, M. M., Goswami, R., Cheng, S. F., Mulvaney, S. P. & Whitman, L. J. (2003). *J. Appl. Phys.* **94**, 778–783.
Chakrapany, S. & Singh, C. (2014). *Am. J. Pharmtech. Res.* **4**, 60–69.
Charnock, J. M., Moyes, L. N., Pattrick, R. A. D., Mosselmans, J. F. W., Vaughan, D. J. & Livens, F. R. (2003). *Am. Miner.* **88**, 1197–1203.
Chaudhary, A. (2011). *J. Biomed. Nanotechnol.* **7**, 68–69.
Chuu, J. J., Liu, S. H. & Lin Shiau, S. Y. (2007). *Toxicol. Lett.* **169**, 109–120.
Colombo, M. J., Ha, J., Reinfelder, J. R., Barkay, T. & Yee, N. (2013). *Geochim. Cosmochim. Acta*, **112**, 166–177.
Colombo, M. J., Ha, J., Reinfelder, J. R., Barkay, T. & Yee, N. (2014). *Chem. Geol.* **363**, 334–340.
De, A. K. (2009). *Environmental Chemistry*, 5th ed., p. 100. New Delhi: New Age International Publishers.
De Jong, W. H. & Borm, P. J. A. (2008). *Intl J. Nanomed.* **3**, 133–149.
Deneen, J. & Carter, C. B. (2006). *Microsc. Microanal.* **12**, 594.
Dubey, N., Dubey, N., Mehta, R. S., Saluja, A. K. & Jain, D. K. (2009). *Songklanakarin J. Sci. Technol.* **31**, 501–510.
Dwivedi, V., Anandan, E. M., Mony, R. S., Muraleedharan, T. S., Valiathan, M. S., Mutsuddi, M. & Lakhotia, S. C. (2012). *PLoS ONE*, **7**, e37113.
Dwivedi, V., Tiwari, S. & Lakhotia, S. C. (2014). *J. Biosci.* **40**, 1–17.
Dwivedi, V., Tripathi, B. K., Mutsuddi, M. & Lakhotia, S. C. (2013). *Curr. Sci.* **105**, 1711–1723.
Frawlay, D. (2000). *Ayurvedic Healing: A Comprehensive Guide.* Twin Lakes: Lotus Press.
Ghosh Chaudhuri, R. & Paria, S. (2012). *Chem. Rev.* **112**, 2373–2433.
Gokarn, R. A., Patgiri, B., Galib & Prajapati, P. K. (2012). *Intl J. Pharm. Bio. Arch.* **3**, 1360–1367.
Hariprapannaji, V. P. (2004). *Rasayogasagara*, Rasasinduram, Sloka 522–524. Varanasi: Chowkhamba Krishnadas Acadamy.
Huang, C.-F., Hsu, C. J., Liu, S. H. & Lin-Shiau, S. Y. (2012). *J. Biomed. Biotech.* **2012**, 254582.
Huggins, F. E., Raverty, S. A., Nielsen, O. S., Sharp, N. E., Robertson, J. D. & Ralston, N. V. C. (2009). *Environ. Bioindic.* **4**, 291–302.
Ingole, R. K. (2013). *Ayurlog Natl J. Res. Ayur. Sci.* **1**, 1–3.
Kamath, S. U., Pemiah, B., Sekar, R. K., Krishnaswamy, S., Sethuraman, S. & Krishnan, U. M. (2012). *Arch. Toxicol.* **86**, 831–838.
Kanojia, A., Sharma, A., Urimindi, V. & Goecha, V. K. (2013). *Intl Ayur. Med. J.* **1**, 1–4.
Karkare, M. & Bahuguna, R. (2007). *Applied Physics I*, p. 39. New Delhi: I. K. International.
Kim, C. S., Rytuba, J. J. & Brown, G. E. Jr (2004). *Appl. Geochem.* **19**, 379–393.
Koch, I., Moriarty, M., Sui, J., Rutter, A., Saperc, R. B. & Reimer, K. J. (2013). *Sci. Tot. Environ.* **454–455**, 9–15.
Koningsberger, D. C. & Prins, R. (1988). *X-ray Absorption: Principles, Applications and Techniques of EXAFS, SEXAFS and XANES.* New York: Wiley.
Krishnamachary, B. J., Rajendran, N., Pemiah, B., Krishnaswamy, S., Krishnan, U. M., Sethuraman, S. & Sekar, K. (2012). *J. Ethnopharmacol.* **142**, 98–104.
Kulkarni, S., RaghavendraRao, N. G. & Narasimhareddy, D. (2013). *Int. Res. J. Pharm.* **4**, 189–192.
Kumar, G. & Gupta, Y. K. (2011). *Ayu*, **33**, 569–575.
Kumar, A., Nair, A. G. C., Reddy, A. V. R. & Garg, A. N. (2006). *J. Radioanal. Nucl. Chem.* **270**, 173–180.
Lahiri, D. (2016). *Physica C*, **436**, 32–37.
Leonti, M. & Casu, L. (2013). *Front. Pharmacol.* **4**, 92.

Liao, H., Nehl, C. L. & Hafner, J. H. (2006). *Nanomedicine*, **1**, 201–208.
Liu, J., Shi, J. Z., Yu, L. M., Goyer, R. A. & Waalkes, M. P. (2008). *Exp. Biol. Med.* **233**, 810–817.
Mahdihassan, S. (1987). *Ind. J. Hist. Sci.* **22**, 63–70.
Manceau, A. & Nagi, K. L. (2008). *Dalton Trans*, **11**, 1421–1425.
Mercury Study Report to Congress (1997). *Health effects of Mercury and Mercury Compounds*, Report EPA-452/R-97–007, Volume V. US Environmental Protection Agency.
Mishra, B., O'Loughlin, E. J., Boyanov, M. I. & Kemner, K. M. (2011). *Environ. Sci. Technol.* **45**, 9597–9603.
Morris, C. G. (1992). *Academic Press Dictionary of Science and Technology*, p. 1350. Oxford: Gulf Professional Publishing.
Mukherjee, I., Senapati, S., Mitra, D., Rakshit, A. K., Das, A. R. & Moulik, S. P. (2010). *Colloids Surf. A*, **360**, 142–149.
Myneni, S. C., Mishra, B. & Fein, J. (2009). *Role of Sulfhydryl Sites on Bacterial Cell Walls in the Biosorption, Mobility and Bioavailability of Mercury and Uranium*, Technical Report DOE-PRINCETON-64518, http://www.osti.gov/scitech/biblio/1111104.
Nandha, R. & Singh, H. (2013). *Intl J. Green Pharm.* **7**, 173–176.
Newville, M. (2001). *J. Synchrotron Rad.* **8**, 96–100.
Newville, M., Ravel, B., Haskel, D., Rehr, J. J., Stern, E. A. & Yacoby, Y. (1995). *Physica B*, **208–209**, 154–156.
Niikura, K., Matsunaga, T., Suzuki, T., Kobayashi, S., Yamaguchi, H., Orba, Y., Kawaguchi, A., Hasegawa, H., Kajino, K., Ninomiya, T., Ijiro, K. & Sawa, H. (2013). *ACS Nano*, **7**, 3926–3938.
Nishteswar, K. (2013). *Ayu*, **34**, 4–5.
Panda, A. K. & Hazra, J. (2012). *Intl J. Res. Ayur. Pharm.* **3**, 772–776.
Panghal, M., Arya, V., Yadav, S., Kumar, S., Yadav, J. P. J. (2010). *Ethnobiol. Ethnomed.* **6**, 1–11.
Patel, N. G. (1986). *Folk Medicine: The Art and the Science*, edited by R. P. Steiner, p. 41. Washington: American Chemical Society.
Patgiri, B. & Gokarn, R. (2014). *Ayurpharm. Intl J. Ayurveda Alli. Sci.* **3**, 41–47.
Patty, C., Barnett, B., Mooney, B., Kahn, A., Levy, S., Liu, Y., Pianetta, P. & Andrews, J. C. (2009). *Environ. Sci. Technol.* **43**, 7397–7402.
Patwabardhan, B. (2011). *J. Ayurveda Integr. Med.* **2**, 47–48.
Paur, I., Carlsen, M. H., Halvorsen, B. L. & Blomhoff, R. (2011). In *Herbal Medicine: Biomolecular and Clinical Aspects*, 2nd ed., edited by I. F. F. Benzie. Wachtel-Galor: CRC Press.
Perrey, C. R., Deneen, J. & Carter, C. B. (2005). *Microscopy of Semiconducting Materials, Springer Proceedings in Physics*, Vol. 107, pp. 315–318.
Petkov, V. (1989). *J. Appl. Cryst.* **22**, 387–389.
Raha, S. (2013). *J. Ayurveda Integr. Med.* **4**, 198–205.
Rajan, M., Darrow, J., Hua, M., Barnett, B., Mendoza, M., Greenfield, B. K. & Andrews, J. C. (2008). *Environ. Sci. Technol.* **42**, 5568–5573.
Rastogi, S. (2010). *Intl J. Ayurveda Res.* **1**, 41–46.
Raut, N. B., Tiwari, U. L., Adhikari, B. S., Rawat, G. S. & Chandola, S. (2013). *Not. Sci. Biol.* **5**, 175–182.
Rickard, D. (2012). *Sulphidic Sediments and Sedimentary Rocks*, p. 178. Amsterdam: Elsevier,
Saper, R. B., Kales, S. N., Paquin, J., Burns, M. J., Eisenberg, D. M., Davis, R. B. & Phillips, R. S. (2004). *J. Am. Med. Assoc.* **23**, 2868–2873.
Sarkar, P. K. & Chaudhury, A. (2010). *J. Sci. Ind. Res.* **69**, 901–905.
Sarkar, P. K., Das, S. & Prajapati, P. K. (2010). *Ancient Sci. Life*, **29**, 1–6.
Sharma, S. (1979*a*). *Rasatarangini*, Sloka 27–30, edited by D. Sastri, p. 79. Varanasi: Motilal Banarasidas.
Sharma, S. (1979*b*). *Rasatarangini*, Sloka 7–12, edited by D. Sastri, p. 176. Varanasi: Motilal Banarasidas.
Sharma, S. (1979*c*). *Rasatarangini*, Sloka 107, edited by D. Sastri, p. 124. Varanasi: Motilal Banarasidas.
Shastry, K. N. (1979). *Rasatarangini.* Varanasi: Motilal Banarasidas Press. (English translation of original in Sanskrit.)
Shibata, T., Bunker, B. A., Zhang, Z., Meisel, D., Vardeman, C. F. & Gezelter, J. D. (2002). *J. Am. Chem. Soc.* **124**, 11989–11996.
Sin, Y. M., Teh, W. F. & Wong, M. K. (1989). *Bull. Environ. Contam. Toxicol.* **42**, 307–314.
Singh, S. K., Chaudhary, A., Rai, D. K., Rai, S. B. (2009). *Ind. J. Trad. Knowl.* **8**, 346–351.
Singh, R., Gautam, N., Mishra, A. & Gupta, R. (2011). *Ind. J. Pharmacol.* **43**, 246.
Smith, D. M., Simon, J. K. & Baker, J. R. Jr (2013). *Nat. Rev. Immunol.* **13**, 592–606.
Svensson, M., Düker, A. & Allard, B. (2006). *J. Hazard. Mater.* **136**, 830–836.
Svoboda, R. E. (1998). *Prakriti: Your Ayurvedic Constitution*, p. 169. Bellingham: Sadhana Publications.
Tabakova, N., Tabakova, S., Beshkov, V., Pojarlieff, I. & Mircheva, V. (2006). *Proceedings of the SGEM2006 Conference*, 12–16 June 2006, Vol. 1, pp. 325–336 (http://sgem.org/sgemlib/spip.php?article1521).
The Ayurvedic Formulatory of India (2003). *The Ayurvedic Formulatory of India*, 2nd ed., Vol. I, Part B, p. 112. New Delhi Department of AYUSH, Government of India, India.
Tiwari, A. & Tiwari, A. (2013). *Bioengineered Materials.* London: Taylor and Francis.
Varier, V. P. S. (1999). *Chikitsa Samgraham*, 15th ed., pp. 148–150. Arya Vaidya Sala, Kottakkal, India.
Valiathan, M. S. (2006). *Curr. Sci.* **90**, 5–6.
Vardhini, N. V., Sathya, T. N. & Balakrishna Murthy, P. (2010). *Curr. Sci.* **99**, 1096–1100.
Wadekar, M. P., Rode, C. V., Bendale, Y. N., Patil, K. R. & Prabhune, A. A. J. (2005). *Pharm. Biomed. Anal.* **39**, 951–955.
Walkey, C., Sykes, E. A. & Chan, W. C. W. (2009). *Hematology*, **2009**, 701–707.
Wang, Q., Kim, D., Dionysiou, D. D., Soriyal, G. A., Timberlake, D. (2004). *Environ. Pollut.* **131**, 323–336.
Wiberg, E. & Wiberg, N. (2001). *Inorganic Chemistry*, p. 1314. New York: Academic Press.
Yeoh, T. S., Lee, A. S. & Lee, H. S. (1986). *Toxicology*, **41**, 107–111.
Yonezawa, T., Onoue, S. & Kimizuka, N. (2000). *Langmuir*, **16**, 5218–5220.
Yoshitomi, T., Miyamoto, D. & Nagasaki, Y. (2009). *Bio-Macromolecules*, **10**, 596–601.
Zhang, L. & Wong, M. H. (2007). *Environ. Intl*, **33**, 108–121.
Zhou, X., Wang, L., Sun, X., Yang, X., Chen, C., Wang, Q. & Yang, X. (2011). *J. Ethnopharmacol.* **135**, 110–115.